EXPERIMENTAL STUDY OF THE BREAKING WAVE IMPACT ON RIGID AND ELASTIC PLATES

Zhengyu Hu, National University of Singapore, z.hu@u.nus.edu
Yuzhu Li, National University of Singapore, pearl.li@nus.edu.sg

INTRODUCTION

Coastal and offshore deformable structures such as flexible breakwaters, wave energy converters, and Floating Production Storage and Offloading (FPSO) hulls are vulnerable to ocean hydrodynamic loads, as structural deformation may happen in these interactions. The structural deformation can lead to decreased wave reflection, wave loading, and runup on the steep-fronted coastal structures in non-breaking waves (Hu et al., 2023; Hu and Li, 2023a). When flexible structures face breaking waves, their structural integrity is challenged. Tremendous impact pressure with a short duration can be produced when water waves are close to or directly break on the structures, which were observed to cause failure cases in practical engineering (Oumeraci, 1994; Tanimoto and Takahashi, 1994). Most previous studies have been devoted to the violent breaking wave impacts on rigid structures (Bullock et al., 2007; Ravindar and Sriram, 2021). Therefore, the understanding of hydroelasticity in the breaking wave impact is still lacking. Hu and Li (2023b) investigated four distinctive breaking wave impacts on a flexible wall using a fully coupled computational model. However, detailed laboratory experiments of breaking wave impact on elastic structures are still required to reveal the mechanics.

In this study, we aim to investigate the breaking wave impact on rigid and elastic plates by a small-scale laboratory experiment. The wave surface elevation, impact pressure, free surface profiles, and structural response subjected to the *high-aeration* impact are presented.

EXPERIMENTAL SETUP

We conducted the laboratory experiments in a wave flume (38 m long, 0.9 m wide, and 0.9 m high) in the hydraulic engineering laboratory at the National University of Singapore. The wave flume is equipped with a 5-m long-stroke piston-type wavemaker on one end and a 1:9.6 glass plane beach on the other end, as sketched in Figure 1. The Cartesian coordinate system is built with the x-axis pointing toward the on-shore direction and the z-axis toward the vertical direction. The origin of the coordinate system is located at the toe of the beach. The solitary wave is generated using Grimshaw's third-order analytical solution for the free surface profile (Grimshaw 1971). The *high-aeration* impact is examined in the present study: the ratio of incident wave height H and offshore water depth h is 0.35, where $h = 0.26$ m. Four capacitance wave gauges located at $x = -2.5$, 0, 1.4, and 1.9 m are used to measure the wave surface elevation at a sampling rate of 200 Hz. A vertical cantilever plate made of Polymethyl methacrylate (PMMA) with 0.38 m in length l and 0.895 m in width w is mounted at $x = 2.4$ m. The Young's modulus E and the density ρ of the plate are 2.9 GPa and 1190 kg/m^3, respectively. Two different plate thicknesses b are designed, i.e., $b = 0.02$ and 0.003 m representing the rigid and elastic cases, respectively. Wave impact pressures were recorded at ten locations on the plate, i.e., from 0.02 to 0.20 m from the fixed end with an interval of 0.02 m by the ATM.1ST analogy pressure sensors at a sampling frequency of 20,000 Hz. The free surface profiles of the breaking wave and free-end displacements of the elastic plate are captured by a high-speed Phantom LAB340 camera at a frame rate of 200 fps.

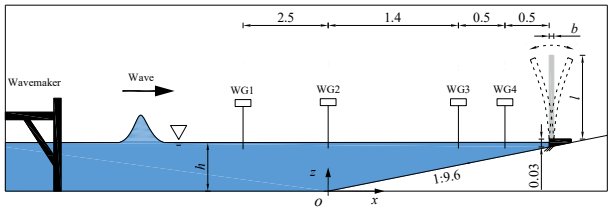

Figure 1 - Sketch of the experimental setup (not to scale)

WAVE SURFACE ELEVATION

Figure 2 shows the wave surface elevation η in front of the rigid and elastic plates at different locations. The incident wave profiles of the two cases perfectly collapse in a single line, indicating the wavemaker can generate repeatable breaking wave impact. Compared to the rigid case, the wave reflection is slightly reduced due to the deflection of the elastic plate, as shown in WG3 and WG4. As the reflected wave propagates in the off-shore direction, the amplitude for the elastic-plate case can be higher than the rigid-plate case due to the wave dispersion, as shown in WG1 and WG2. Subsequently, slight differences in the wave surface elevation are observed between these two cases during the vibration of the elastic plate.

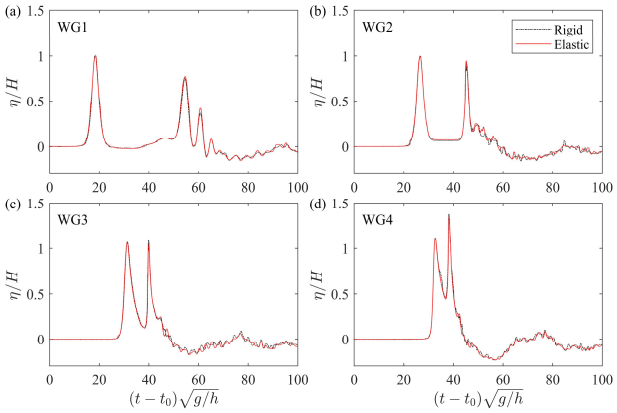

Figure 2 - Wave surface elevation in front of the rigid and elastic plates

IMPACT PRESSURE

Figure 3 shows the spatial distribution of the peak pressure p_{max} along the rigid and elastic plates subjected to the *high-aeration* impact, where p_0 is the standard atmospheric pressure. The impact point is located at $(z-h)/l = 0.22$, which will be shown in Figure 4a. The maximum peak pressure spreads within the entrapped-air region beneath the impact point for both cases. The measured peak pressures are distributed evenly in this region. They are very close between the rigid and elastic plates as the negligible deflection appears near the fixed end. The peak pressure decreases above the impact point, especially for the elastic-plate case. With the increasing structural deflection, p_{max} on the elastic plate, determined by the quasi-hydrostatic pressure, is slightly higher than that on the rigid plate when $(z-h)/l > 0.37$. This is because more fluid runs up the inclined deformed plate.

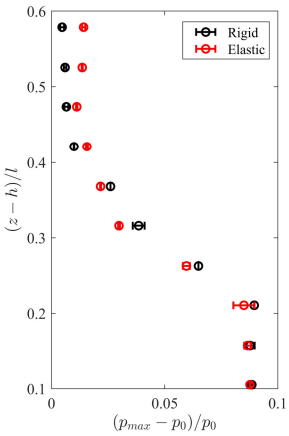

Figure 3 - Impact pressures along the rigid and elastic plates

STRUCTURAL RESPONSE

Figure 4 shows the free surface profiles and the corresponding free-top displacement D_x of the elastic plate subjected to the *high-aeration* impact. In Figure 4a, a large air pocket is entrapped between the overturning wavefront and the plate face at the impact instant. The structural displacement is initialized by the impact pressure. In Figure 4b, as the wave shoots up the deformed plate, the elongated air pocket breaks into a series of air bubbles. At this time instant, D_x reaches a peak value. As the air bubbles evolve, high-frequency vibrations are excited with a mean deflection of $0.05l$. Its frequency is larger than the natural frequency of the elastic plate in vacuo. Subsequently, the majority of air bubbles escaped from the wave tongue, as shown in Figure 4c. At this time instant, the largest free-top displacement $D_x = 0.11l$ occurs under the maximum quasi-hydrostatic force during the wave run-down phase. Under the restoration force, the elastic plate then deflects toward the off-shore direction. Finally, the elastic wall vibrates at its natural frequency with a decreasing amplitude, which is consistent with the results of Hu and Li (2023b).

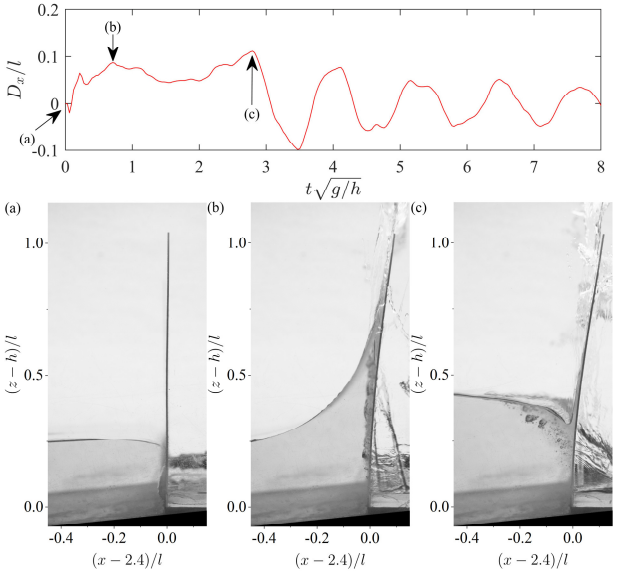

Figure 4 - Free surface profiles and the corresponding structural horizontal displacement

CONCLUSION

In this study, we have investigated the *high-aeration* impact on rigid and elastic plates through laboratory experiments. Compared to the rigid-plate case, the high-frequency oscillations in the free surface and the maximum quasi-hydrostatic pressure above the impact region are affected by structural deformation. However, the negligible plate deflection near the fixed end has a minor influence on the impact pressure. After the breaking wave impact, the evolution of the entrapped air pocket plays a critical role in the structural vibration. This study provides insights into the hydroelasticity in breaking wave impacts and a database for the validation of simulations.

REFERENCES

Bullock, G.N., Obhrai, C., Peregrine, D.H. and Bredmose, H. (2007): Violent breaking wave impacts. Part 1: Results from large-scale regular wave tests on vertical and sloping walls. Coast. Eng., vol. 54, pp. 602-617.

Bredmose, H., Peregrine, D.H. and Bullock, G.N. (2009): Violent breaking wave impacts. Part 2: Modelling the effect of air. J. Fluid Mech., vol. 641, pp. 389-430.

Grimshaw, R. (1971): The solitary wave in water of variable depth. Part 2. J. Fluid Mech., vol. 46, pp. 611-622.

Hu, Z., Huang, L. and Li, Y. (2023): Fully-coupled hydroelastic modeling of a deformable wall in waves. Coast. Eng., vol. 179, pp. 104245.

Hu, Z. and Li, Y. (2023a): Numerical study on the interaction between periodic waves and a flexible wall. Coastal Engineering Proceedings, pp. structures.3.

Hu, Z. and Li, Y. (2023b): Two-dimensional simulations of large-scale violent breaking wave impacts on a flexible wall. Coast. Eng., vol. 185, pp. 104370.

Oumeraci, H. (1994): Review and analysis of vertical breakwater failures – lessons learned. Coast. Eng., vol. 22, pp. 3-29.

Tanimoto, K. and Takahashi, S. (1994): Design and construction of caisson breakwaters – the japanese experience. Coast. Eng., vol. 22, pp. 57-77.